Volume 27
Number 17
7 May 2025
Pages 8577–9286

PCCP

Physical Chemistry Chemical Physics

rsc.li/pccp

25 YEARS ANNIVERSARY

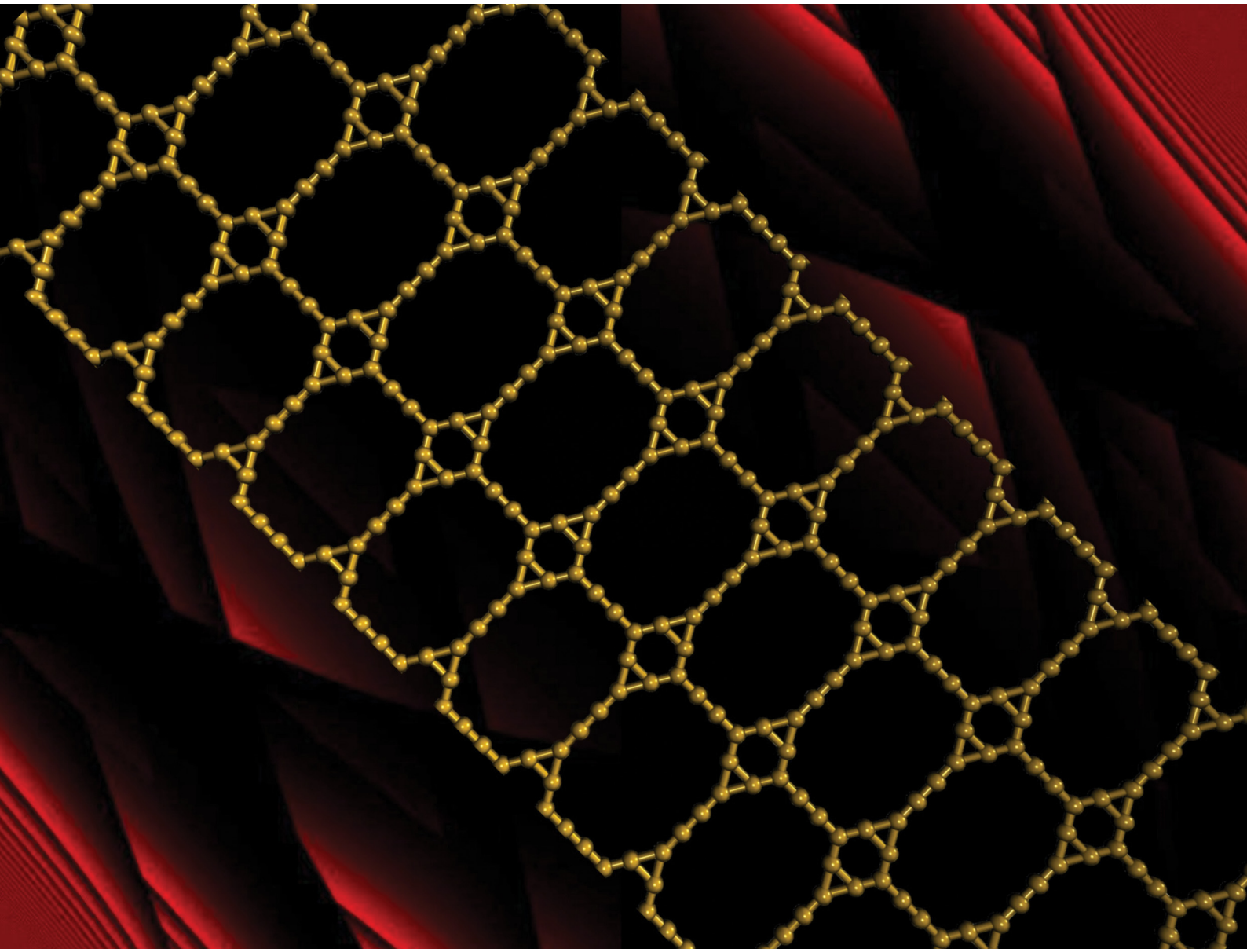

ISSN 1463-9076

ROYAL SOCIETY OF CHEMISTRY

PAPER
Marcelo L. Pereira *et al.*
TH-graphyne: a new porous bidimensional carbon allotrope

PCCP Owner Societies

PCCP

ROYAL SOCIETY OF CHEMISTRY

PAPER

Published on 11 September 2024
Licence and permissions

Check for updates

Cite this: *Phys. Chem. Chem. Phys.*, 2025, **27**, 8684

TH-graphyne: a new porous bidimensional carbon allotrope

Kleuton A. L. Lima,[ab] Rodrigo A. F. Alves,[ab] Daniel A. da Silva,[c] Fábio L. L. Mendonça,[d] Marcelo L. Pereira Jr *[d] and Luiz A. Ribeiro Jr [ab]

Received 23rd July 2024,
Accepted 5th September 2024

DOI: 10.1039/d4cp02923b

rsc.li/pccp

Graphyne and two-dimensional porous carbon-based materials have garnered significant attention due to their interesting structural characteristics and essential properties for new technological applications. Within this scope, this work investigates the structural, thermal, electronic, optical, and mechanical properties of a novel two-dimensional allotrope that combines triangular (T) and hexagonal (H) rings, connected by acetylenic linkages (graphyne-like), thus named TH-graphyne (TH-GY). This study comprehensively characterizes the proposed system's behavior using density functional theory, *ab initio* molecular dynamics, and classical reactive molecular dynamics simulations. Our results confirm the structural stability of TH-GY. AIMD simulations demonstrate the material's thermal stability at elevated temperatures, while phonon dispersions indicate its dynamical stability. Electronic band structure calculations show that the system is metallic. The analysis of optical properties reveals intense activity in the visible and UV regions, with pronounced anisotropy. A machine learning interatomic potentials model was developed for TH-GY and used to determine the mechanical behavior of the system, which exhibits Young's modulus ranging from 263 to 356 GPa, highlighting its flexibility. Classical reactive MD simulations elucidate the fracture behavior of TH-GY, revealing distinct fracture patterns and mechanical anisotropy.

1 Introduction

Two-dimensional (2D) carbon-based materials have garnered significant interest from the scientific community due to their intrinsic properties[1,2] and potential applications in new technologies,[3] depending on their atomic arrangement. Graphene, a 2D sheet of sp^2-hybridized carbon arranged in a honeycomb lattice, remains this class's most important and investigated material, particularly since its synthesis in 2004.[4] It possesses high mechanical strength, thermal and electrical conductivity, and optical transparency,[5–7] which are crucial characteristics for driving innovations in various fields, including electronics,[8,9] photonics,[10] energy storage,[11] and biomedical applications.[12] The ability to manipulate graphene at the atomic scale has led to the development of various nanostructures and heterostructures, fueling the search for new materials with specific properties for different applications.[13] Computational materials science is fundamental in this endeavor. It provides insights into the structure–property relationships of 2D carbon-based materials and guides their design for the next generation of new technologies.[14,15]

Recent advances in synthesis techniques have expanded the scope of carbon allotropes beyond graphene, revealing the rich landscape of graphyne derivatives.[16] γ-Graphyne, characterized by sp-hybridized carbon networks with diverse ring topologies,[17] offers promising prospects for tuning electronic, mechanical, and chemical properties.[18] These advances in synthesis processes have paved the way for exploring new carbon allotropes with distinct structural motifs and functionalities.[19]

The rapid expansion of computational methods for predicting the properties of 2D carbon-based materials also represents a significant pathway for anticipatory materials design.[20] Notable examples include the prediction of biphenylene network,[21] fullerene monolayer,[22] and γ-graphyne,[23] decades before their experimental realization.[24–29] These computational insights enable researchers to explore vast regions of the materials landscape, accelerating the discovery of new carbon allotropes with tailored properties and applications.[30]

Within the class of carbon-based nanomaterials, those with porous structural characteristics offer diverse applications, ranging from gas separation and storage[31] to catalysis.[32] With high surface area[33] and versatility,[34] these systems are of interest for addressing social and environmental challenges through new technologies.[35] In this context, we propose a new 2D porous carbon-based material, TH-graphyne (TH-GY—where T and

[a] *University of Brasília, Institute of Physics, Brasília, Federal District, Brazil*
[b] *Computational Materials Laboratory, LCCMat, Institute of Physics, University of Brasília, Brasília, Federal District, Brazil*
[c] *Professional Postgraduate Program in Electrical Engineering (PPEE), Department of Electrical Engineering, College of Technology, University of Brasília, Brasília, Federal District, Brazil*
[d] *Department of Electrical Engineering, University of Brasília, Brasilia, Federal District, Brazil. E-mail: marcelo.lopes@unb.br*

H represent its composition with triangular and hexagonal carbon rings, respectively), as a promising addition to this growing class of materials. This system can be helpful in fields such as membrane technology, energy storage, sensors, and molecular separation.

In this work, we employ density functional theory (DFT), *ab initio* molecular dynamics (AIMD), and classical reactive molecular dynamics (MD) simulations to discuss the electronic and structural properties of TH-GY. We present its intrinsic characteristics as a new 2D porous carbon allotrope through theoretical investigations. Our study verifies its structural integrity, indicated by the absence of imaginary frequencies in the phonon spectrum, as well as its thermal stability at temperatures up to 1000 K. Regarding its electronic characteristics, TH-GY exhibits metallic behavior, with significant optical activity in the visible and ultraviolet ranges, and a Young's modulus ranging from 263 to 356 GPa, depending on the direction of applied strain.

2 Methodology

We combined classical and first-principles computational approaches to investigate the structural, thermal, electronic, optical, and mechanical properties of TH-GY. Fig. 1(c) presents the system's lattice structure. DFT calculations, including AIMD, were conducted using the CASTEP code within the Biovia Materials Studio software.[36,37] We employed the generalized gradient approximation (GGA) with the Perdew–Burke–Ernzerhof (PBE)[38] and Heyd–Scuseria–Ernzerhof hybrid (HSE06)[39] functionals to describe the exchange–correlation effects accurately. Norm-conserving pseudopotentials were used to account for electron-nucleus interactions and electronic self-consistency was achieved using the iterative non-linear Broyden–Fletcher–Goldfarb–Shanno (BFGS) algorithm.[40,41]

The plane wave basis set with an energy cutoff of 500 eV ensured accurate electronic structure calculations, with convergence criteria set for energy and forces of 1.0×10^{-5} eV and 1.0×10^{-3} eV Å^{-1}, respectively. Structural relaxation employed periodic boundary conditions, ensuring minimal residual forces and pressure below 0.01 GPa. To avoid interaction between TH-GY layers, the vacuum space was set to 10 Å in the out-of-plane direction. Phononic characteristics were analyzed using a linear response method. Electronic and optical calculations utilized a *k*-point grid of $15 \times 15 \times 1$ for the PBE

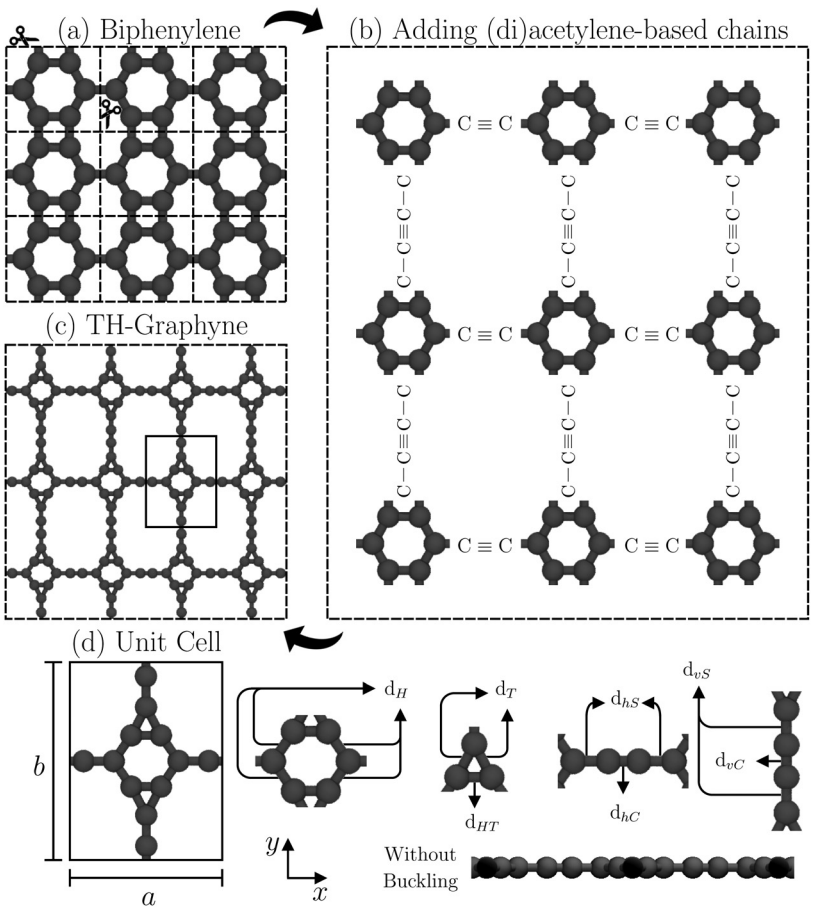

Fig. 1 Schematic representation of the motivation and structure of TH-GY. The system is based on the recently synthesized biphenylene network (a), with hexagons kept intact, acetylenes inserted horizontally, and diacetylenes inserted vertically (b). The structure formed by these changes is TH-GY (c). In its unit cell (d), seven different types of bonds can be identified: those exclusive to the hexagons (d_H), exclusive to the triangles (d_T), triangle–hexagon connections (d_{HT}), the central bonds of the horizontal acetylene (d_{hC}) and vertical diacetylene (d_{vC}), and the supporting bonds of the horizontal acetylene (d_{hC}) and vertical diacetylene (d_{vC}). A side view of the system is presented at the bottom of the figure, showing that TH-GY is a planar material.

method and 5 × 5 × 1 for the HSE06 method, respectively. The partial density of states (PDOS) was calculated at the HSE06 level using a *k*-point grid of 20 × 20 × 1. Optical properties were explored under an external electric field using complex dielectric constant calculations.[42] To investigate the thermal stability of TH-GY, AIMD simulations were conducted at a temperature of 1000 K. A Nosé–Hoover thermostat[43] was employed for precise temperature control, with a fixed time step of 1.0 fs during a total simulation duration of 5 ps in a canonical (NVT) ensemble. In these calculations, a 2 × 2 × 1 supercell with 48 atoms was considered. This methodology is consistent with studies in the literature.[44,45]

The mechanical behavior of TH-GY was investigated through classical reactive molecular dynamics simulations using the LAMMPS (large-scale atomic/molecular massively parallel simulator) software.[46]

A reactive force field specifically developed for TH-GY was obtained from a moment tensor potential (MTP),[47] fitted to investigate mechanical properties with the assistance of the MLIP package.[48] AIMD simulations were conducted again, with the same parameters described for this protocol, utilizing the Vienna ab initio simulation package (VASP).[49] The training dataset for the MLIPs was prepared using stress-free and uniaxially strained supercells under various temperatures. Notably, this approach has recently been successfully employed to generate MLIPs.[50–53] An MTP with a cutoff distance of 3.5 Å was trained using the two-step passive training approach, as considered in recent studies.[50–54]

The velocity Verlet algorithm integrated Newtons equations of motion with a time step of 0.05 fs,[55] while thermalization and stress relief were achieved through thermostat and NPT simulations for 100 ps.[56] Elastic properties and fracture patterns were assessed at 300 K, with the TH-GY sheet stretched using a constant engineering tensile strain rate of 10^{-6} fs^{-1}.

For the strain calculation as a function of the applied deformation, we computed the stress tensor for each atom *i*, given by $S_{aa} = -mv_a^2 - W_{aa}$ divided by the volume, where *a* can be *x* or *y*, depending on the evaluated direction. Here, *m* is the atom's mass, v_a is the velocity in the corresponding direction, and *W* represents the virial contribution due to intra- and intermolecular interactions.[57] Since it is a two-dimensional system, the volume is given by $V = L_xL_yh_0$, where h_0 corresponds to the system's thickness, and L_x and L_y denote the lengths in the *x* and *y* directions, respectively. Given that it is a monolayer system, h_0 was considered to be 3.35 Å, corresponding to the graphene thickness.[58] The strain is dependent on the system size, defined as $\varepsilon_{x,y} = (L_{x,y} - L_{x,y}{}^0)/L_{x,y}{}^0$, where $L_{x,y}{}^0$ is the initial length of the system in the evaluated direction after the equilibration steps.

3 Results

The motivation behind constructing TH-GY is similar to the approach to derive γ-graphyne from graphene.[27] Fig. 1 illustrates the logical sequence of this construction from panels (a) to (c). By maintaining the hexagons intact, acetylene and diacetylene were introduced along the *x* and *y* directions, respectively. The choice to insert diacetylene in the *y* direction was made to preserve the intrinsic sp-type bonding characteristic, as the outermost carbon atoms were part of the triangular ring, resulting in sp^2 hybridized bonds. Similar strategies for creating new carbon allotropes based on known systems are commonly reported in the literature.[59,60] Recently, Jenkins *et al.* proposed THD-C, which incorporates acetylene between consecutive chains in the biphenylene network, preserving not only the hexagonal ring but also the rectangular one.[61] In another study, Ullah, Menezes, and Silva proposed a tolanene carbon allotrope,[62] following the same perspective of connecting biphenylene blocks *via* acetylenes, investigating its electronic and structural properties, and lithium diffusion.

Fig. 1(d) shows the unit cell of TH-GY. From the optimization calculations discussed, the lattice vectors of the system are *a* = 7.02 Å and *b* = 9.13 Å, with lattice angles α = β = γ = 90°,

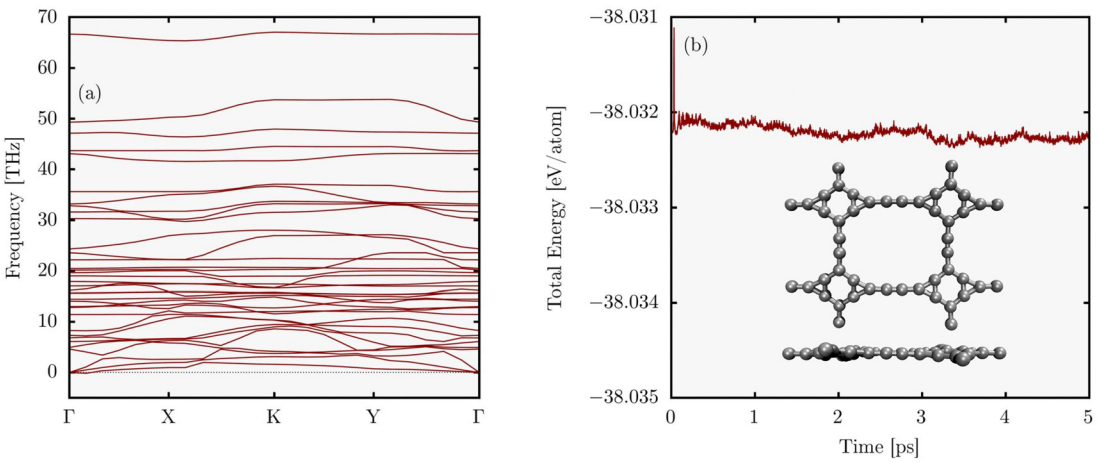

Fig. 2 Calculations regarding the stability of TH-GY: vibrational phonon-mode dispersion (a) and time evolution of the total energy at 1000 K during five ps of simulation (b). The presented structures correspond to the front and side views at the simulation instant.

confirming its crystalline structure within the space group *Pmmm* (D2H-1). The unit cell, composed of 12 atoms, exhibits diagonal symmetry in the *xy* plane and features seven distinct bond lengths. For the bonds unique to the triangular and hexagonal rings, the lengths are d_T = 1.48 Å and d_H = 1.44 Å, respectively. The bond length between hexagon and triangle is d_{HT} = 1.16 Å. The central bond lengths for acetylene and diacetylene are d_{hC} = 1.21 Å and d_{vC} = 1.28 Å, respectively. Finally, the bonds connecting the sp-hybridized pairs are d_{hS} = 1.40 Å and d_{vC} = 1.42 Å for acetylene and diacetylene, respectively. The formation energy of TH-GY is −8.0 eV per atom, which falls within the range of values reported for other 2D carbon allotropes.[3]

In addition to the cohesive energy suggesting that TH-GY is a stable and feasible system, Fig. 2(a) presents the vibrational spectrum of the system. A small dispersion of imaginary frequencies near the Γ point is observed, with a maximum magnitude of 0.1 THz, corresponding to a slight residual compressive strain in the material along the $\Gamma \rightarrow$ X path. This behavior is commonly observed in other carbon-based systems, including graphene multilayers, and can be easily removed with a slight system deformation.[63] All other frequencies in TH-GY are real, indicating the overall stability of the nanomaterial's lattice dynamics. In addition to the system's dynamic stability, the nanomaterial exhibits an isolated dispersion around approximately 65 THz, primarily planar, resulting from vibrations in the d_{hC} and d_{vC} bonds, which are common in systems with sp-type bonds.[61,62,64] Besides this isolated frequency, the maximum dispersion in TH-GY, approximately 49 THz, is close to that reported for biphenylene network.[63] Finally, the absence of a discernible gap between acoustic and optical modes implies significant phonon scattering, potentially leading to shorter phonon lifetimes and moderate thermal conductivity.

Fig. 2(b) provides insights into the thermal stability of TH-GY through AIMD simulations conducted at 1000 K. Using 2 × 2 × 1 supercells with 48 atoms, the time evolution of the total energy was monitored. The constant, flat pattern observed throughout the simulation suggests no reconfiguration of the lattice, bond breaking, or reconstruction within the material. The inset panels further confirm the structural integrity of the nanomaterial and its current form, as no significant changes are observed in the lattice configuration. Additionally, the energy fluctuations are considered negligible, and the system remains essentially flat.

The band structure of TH-GY reveals a distinctive metallic nature of the nanomaterial, as shown in Fig. 3(a). Overlapping bands near the Fermi level characterize this nature. This result indicates a higher ease of electronic delocalization and conduction through the material. The absence of a bandgap in the electronic structure suggests that TH-GY exhibits significantly high electrical conductivity. However, transport calculations on the material still need to be performed to substantiate this claim accurately. Thus, the nanomaterial is a promising candidate for applications requiring high charge carrier mobility, such as transparent conductive coatings and electrodes in electronic devices. Although slight discrepancies in energy dispersion are observed between the PBE and HSE06 calculations, attributed to the known tendency of PBE to underestimate energy levels, both methods closely align in defining the metallic trend exhibited by TH-GY.

Complementing the electronic band structure, Fig. 3(b) presents the partial density of states (PDOS) of TH-GY, providing further insights into its electronic properties. The PDOS reveals the distribution of electronic states across different energy levels, highlighting the contributions of specific atomic orbitals to the overall electronic structure of the nanomaterial. The PDOS exhibits pronounced peaks around 3 eV for the atoms forming the junction between hexagonal and triangular rings, particularly from the p orbital. At approximately 3 eV, the highest concentration of states is related to the third atom of the triangular rings and the atoms between the triangular rings, *i.e.*, the center of the diacetylene, with another concentration of states around −3 eV. Near the Fermi level, there are smaller

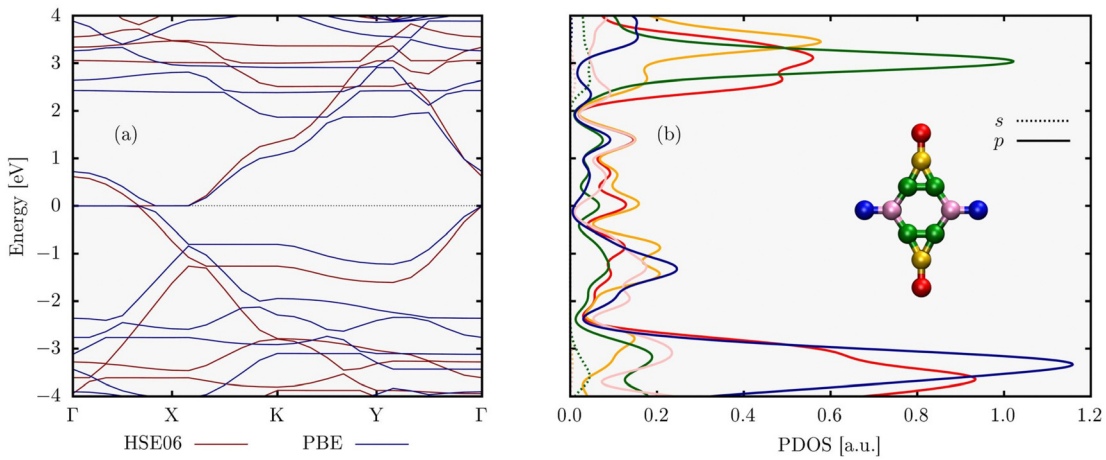

Fig. 3 Electronic band structure (a) was obtained using the PBE (blue curve) and HSE06 (red curve) methods. Partial density of states (PDOS) (b), where the unit cell of TH-GY is highlighted along with the colors representing electronic symmetry.

contributions from these states. The significant contributions of the carbon p orbitals to the electronic states near the band edges further reinforce the metallic behavior observed in the band structure, highlighting the importance of electronic delocalization and strong π-bonding interactions in TH-GY.

Complementing the electronic band structure, Fig. 3(b) presents the partial density of states (PDOS) of TH-GY, providing further insights into its electronic properties. The PDOS reveals the distribution of electronic states across different energy levels, highlighting the contributions of specific atomic orbitals to the overall electronic structure of the nanomaterial. The PDOS exhibits pronounced peaks around 3 eV for the atoms forming the junction between hexagonal and triangular rings, particularly from the p orbital. At approximately 3 eV, the highest concentration of states is related to the third atom of the triangular rings and the atoms between the triangular rings, *i.e.*, the center of the diacetylene, with another concentration of states around −3 eV. Near the Fermi level, there are smaller contributions from these states. The significant contributions of the carbon p orbitals to the electronic states near the band edges further reinforce the metallic behavior observed in the band structure, highlighting the importance of electronic delocalization and strong π-bonding interactions in TH-GY.

To complete the quantum characterization of TH-GY, the optical properties were investigated considering a standard external electric field of 1.0 V Å^{-1} along the x and z directions.[65] Using the Kramers–Kronig relation in conjunction with Fermi's golden rule, the real ε_1 and imaginary ε_2 parts of the dielectric constant are obtained from the following equations:

$$\varepsilon_1(\omega) = 1 + \frac{1}{\pi} P \int_0^{\infty} \mathrm{d}\omega' \frac{\omega' \varepsilon_2(\omega')}{\omega'^2 - \omega^2}, \tag{1}$$

and

$$\varepsilon_2(\omega) = \frac{4\pi^2}{V_\Omega \omega^2} \sum_{i \in \mathrm{VB}, j \in \mathrm{CB}} \sum_k W_k |\rho_{ij}|^2 \delta(\varepsilon_{kj} - \varepsilon_{ki} - \hbar\omega), \tag{2}$$

where P is the Cauchy principal value, W_k is the k-point weight in reciprocal space, ρ_{ij} is the dipole transition matrix element, ω is the photon frequency, and V_Ω is the unit cell volume. VB and CB refer to the valence and conduction bands, respectively.[66]

Once the real and imaginary parts of the dielectric constant are obtained, other relevant optical coefficients, such as the absorption coefficient (α) and reflectivity (R), can be derived as follows:

$$\alpha(\omega) = \sqrt{2}\omega \left[\left(\varepsilon_1^2(\omega) + \varepsilon_2^2(\omega) \right)^{1/2} - \varepsilon_1(\omega) \right]^{1/2}, \tag{3}$$

and

$$R(\omega) = \left[\frac{(\varepsilon_1(\omega) + i\varepsilon_2(\omega))^{1/2} - 1}{(\varepsilon_1(\omega) + i\varepsilon_2(\omega))^{1/2} + 1} \right]^2. \tag{4}$$

Based on the expressions presented above, Fig. 4 discusses the optical properties of TH-GY. This nanomaterial exhibits strong activity in the visible range and, notably, in the infrared (IR) when the field is oriented along the y direction ($E||Y$). In this context, Fig. 4(a) shows an absorption coefficient varying from 1.2 × 10^{-5} cm^{-1} to 0.6 × 10^{-5} cm^{-1} from IR to ultraviolet (UV) when $E||Y$. Additionally, TH-GY exhibits considerable in-plane anisotropy concerning its overall optical properties. The absorption coefficient when the field is oriented along the x direction ($E||X$) remains approximately constant, around 0.3 × 10^{-5} cm^{-1} across the visible range up to UV. The metallic nature of the nanomaterial corresponds to absorption coefficients on the order of 1.0 × 10^{-5} cm^{-1}. The initial absorption peaks for light polarized along $E||X$ and $E||Y$ are located in the infrared and visible spectra (with peaks around 1.3 eV for the x direction and 2.3 eV for the y direction), respectively. This behavior differs from that reported for graphene.[67] Notably, the peak around 1.3 eV aligns with those found in γ-graphyne,[68] suggesting analogous behaviors among these carbon-based materials concerning their absorption properties in the IR.

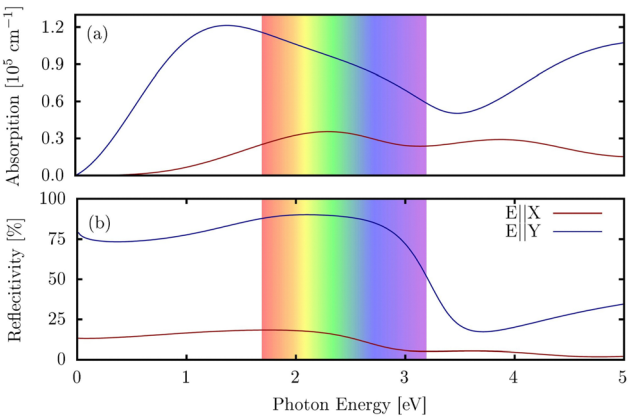

Fig. 4 Absorption coefficient (a) and reflectivity (b) as a function of photon energy for TH-GY.

The mechanical properties and fracture behavior of TH-GY were systematically investigated through classical reactive molecular dynamics simulations using an ML interatomic potential trained explicitly for the nanomaterial. This study provided insights into its structural integrity and fracture patterns under tensile loading in the x and y directions (see Fig. 1). Using a 15 × 11 × 1 supercell of TH-GY with dimensions of 105.15 × 100.42 Å^2 and containing 1980 carbon atoms, with periodic boundary conditions and employing the isothermal–isobaric (NPT) ensemble, we explored the stress–strain dynamics along the x and y directions, as illustrated in Fig. 5. The resulting stress–strain curves revealed distinct mechanical responses between the x and y directions, indicative of the material's anisotropic behavior. TH-GY exhibited a critical strain of 12.0% (9.5%), critical stress of 29.33 GPa (44.76 GPa), and Young's modulus of 188.1 GPa (245.38 GPa) in the x (y) directions. Additionally, the porous structure of TH-GY contributed to its significantly lower Young's modulus compared to γ-graphyne[69] and THD-C,[61] making it less resistant to external stress, though with a greater Poisson's ratio effect.

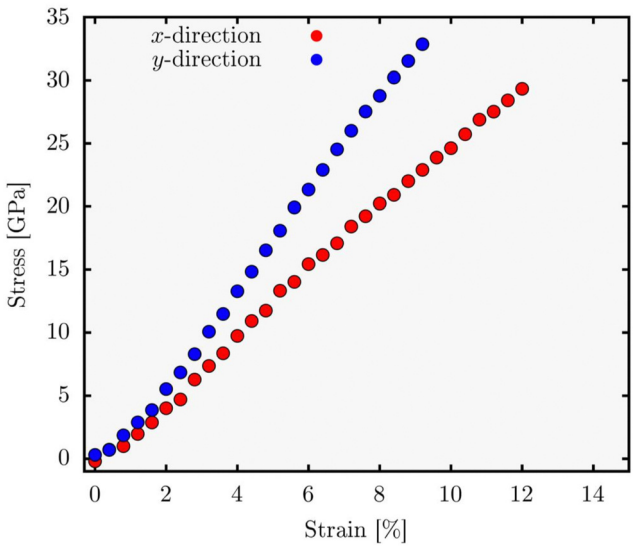

Fig. 5 Stress–strain curves of TH-GY with uniaxial strain in the x- (red) and y-direction (blue), using reactive MD with MLIP.

Exploring the fracture patterns of TH-GY, Fig. 6 provides a comprehensive visual representation of the fracture process under stress in the x and y directions at 300 K, with zero pressure in the direction perpendicular to the deformation. These conditions align with what is typically expected in experiments conducted on 2D materials, where one of the in-plane directions is left free to better understand the nanomaterial's mechanical response in the deformation direction and account for temperature effects (in this case, ambient temperature). The color gradient in the molecular dynamics snapshots corresponds to von Mises (VM) stress per atom,[70–73] calculated from the expression:

$$\sigma^{i}_{\mathrm{VM}} = \sqrt{\frac{(\Delta\sigma_{xy}{}^{i})^2 + (\Delta\sigma_{yz}{}^{i})^2 + (\Delta\sigma_{xz}{}^{i})^2 + 6\left((\sigma_{xy}{}^{i})^2 + (\sigma_{yz}{}^{i})^2 + (\sigma_{zx}{}^{i})^2\right)}{2}}, \tag{5}$$

with $\Delta\sigma_{xy}{}^{i} = \sigma_{xxi}{}^{i} - \sigma_{yy}{}^{i}$, $\Delta\sigma_{yz}{}^{i} = \sigma_{yy}{}^{i} - \sigma_{zz}{}^{i}$, $\Delta\sigma_{xz}{}^{i} = \sigma_{xx}{}^{i} - \sigma_{zz}{}^{i}$, where $\sigma_{xx}{}^{i}$, $\sigma_{yy}{}^{i}$, and $\sigma_{zz}{}^{i}$ are the normal stress components, and $\sigma_{xy}{}^{i}$, $\sigma_{yz}{}^{i}$, and $\sigma_{zx}{}^{i}$ are the shear stress components. The VM offering crucial insights into the initiation and propagation of fractures. Initially, the lattice exhibited elastic behavior, with no structural failure observed. However, beyond critical strains, TH-GY underwent a sudden transition to complete fracture, accompanied by crack propagation along the direction opposite to the applied stress.

In Fig. 6, stress accumulation under deformation in the x direction occurs both in the acetylenes parallel to the direction of deformation and in the hexagons. In contrast, for deformation in the y direction, due to the rigid nature of the triangular rings, stress accumulates primarily in the sp-bonded linkages of the diacetylene, with the hexagons not experiencing significant stress in this case. In both directions, linear atomic chains (LACs) were formed after and near the lattice's fracture region, indicating the plastic stage's onset during tensile loading. These fracture patterns provide valuable insights into the mechanical behavior of TH-GY and offer a basis for understanding its structural stability and fracture mechanisms under external stress conditions.

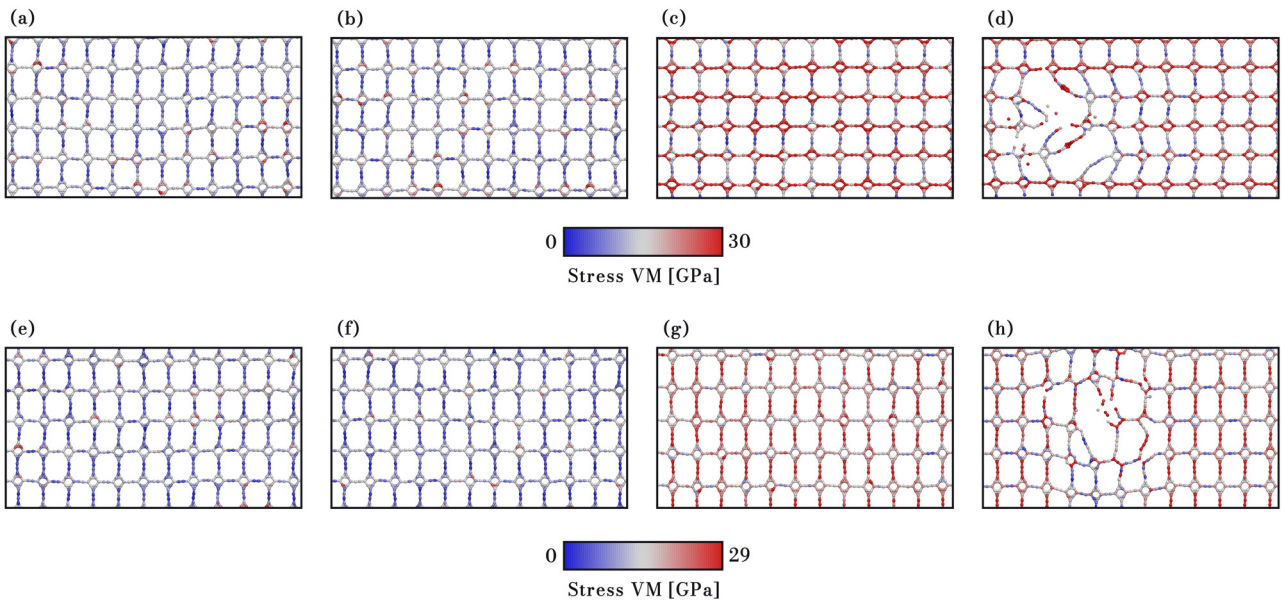

Fig. 6 Illustrations of TH-GY deformation along the x- and y-directions are presented. Panels (a) to (d) showcase deformations of 0%, 1%, 12.0%, and 12.1% along the x axis, respectively, while panels (e) to (h) portray deformations of 0%, 1%, 9.5%, and 9.6% along the y axis, respectively. Atom coloring corresponds to von Mises stress distribution.

4 Conclusion

In conclusion, our study provides a comprehensive investigation into the properties of TH-graphyne, a novel porous 2D carbon allotrope. Using computational techniques, including DFT, AIMD, machine learning-based interatomic potential training, and classical reactive MD simulations, we have elucidated the structural stability, electronic behavior, thermal characteristics, optical properties, and mechanical response of TH-graphyne. Our results confirm the structural integrity of the nanomaterial, with DFT optimizations and AIMD simulations demonstrating its stability under various environmental conditions. Electronic band structure calculations reveal the metallic nature of TH-graphyne, with Young's modulus ranging from 263 to 356 GPa, indicating its lower mechanical strength compared to other two-dimensional allotropes with only sp^2 hybridization due to its high porosity. Optical properties analysis shows intense UV activity and pronounced anisotropy, suggesting potential for tailored optical applications. Additionally, classical reactive MD simulations provide insights into the fracture behavior of TH-graphyne, highlighting its mechanical anisotropy and fracture patterns. Overall, our findings underscore the promising properties of the investigated porous two-dimensional system and its potential for applications in electronics, optoelectronics, and structural materials, paving the way for further exploration and utilization of this intriguing carbon allotrope.

Author contributions

K. A. L. L.: data curation, software, investigation. R. A. F. A.: data curation, investigation, visualization. D. A. S.: data curation, investigation, writing – original draft. F. L. L. M.: investigation, writing – original draft, funding acquisition. M. L. P. J.: conceptualization, methodology, validation, investigation, writing – review & editing, project administration, funding acquisition. L. A. R. J.: conceptualization, validation, formal analysis, investigation, writing – original draft, supervision, project administration, funding acquisition.

Data availability

The data that support the findings of this study are available from the corresponding author, M. L. P. Jr, upon reasonable request.

Conflicts of interest

There are no conflicts to declare.

Acknowledgements

This work received partial support from Brazilian agencies CAPES, CNPq, and FAPDF. M. L. P. J. acknowledges the financial support of the FAP-DF grant 00193-00001807/2023-16. Thanks also to CENAPAD-SP (National High-Performance Center in São Paulo, State University of Campinas – UNICAMP, project: proj960) and NACAD (High-Performance Computing Center, Lobo Carneiro Supercomputer, Federal University of Rio de Janeiro – UFRJ, project: a22002) for the computational support provided. L. A. R. J. L. A. R. J. acknowledges the financial support from FAP-DF 00193.00001808/2022 – 71 and 00193 – 00001857/2023 – 95 grant and FAPDF-PRONEM grant 00193.00001247/2021 – 20, and CNPq grant 350176/2022 – 1.

Notes and references

1 E.-M. Kirchner and T. Hirsch, *Microchim. Acta*, 2020, **187**, 441.
2 R. Majidi and A. I. Ayesh, *Adv. Theory Simul.*, 2024, **7**, 2400131.
3 S. Jana, A. Bandyopadhyay, S. Datta, D. Bhattacharya and D. Jana, *J. Phys.: Condens. Matter*, 2021, **34**, 053001.
4 K. S. Novoselov, A. K. Geim, S. V. Morozov, D.-E. Jiang, Y. Zhang, S. V. Dubonos, I. V. Grigorieva and A. A. Firsov, *Science*, 2004, **306**, 666–669.
5 V. B. Mbayachi, E. Ndayiragije, T. Sammani, S. Taj and E. R. Mbuta, *et al.*, *Results Chem.*, 2021, **3**, 100163.
6 F. Zhang, K. Yang, G. Liu, Y. Chen, M. Wang, S. Li and R. Li, *Composites, Part A*, 2022, **160**, 107051.
7 S. K. Tiwari, S. Sahoo, N. Wang and A. Huczko, *J. Sci.: Adv. Mater. Devices*, 2020, **5**, 10–29.
8 V. Saraswat, R. M. Jacobberger and M. S. Arnold, *ACS Nano*, 2021, **15**, 3674–3708.
9 M. G. Stanford, C. Zhang, J. D. Fowlkes, A. Hoffman, I. N. Ivanov, P. D. Rack and J. M. Tour, *ACS Appl. Mater. Interfaces*, 2020, **12**, 10902–10907.
10 H. Lin, K.-T. Lin, T. Yang and B. Jia, *Adv. Mater. Technol.*, 2021, **6**, 2000963.
11 A. G. Olabi, M. A. Abdelkareem, T. Wilberforce and E. T. Sayed, *Renewable Sustainable Energy Rev.*, 2021, **135**, 110026.
12 M. Derakhshi, S. Daemi, P. Shahini, A. Habibzadeh, E. Mostafavi and A. A. Ashkarran, *J. Funct. Biomater.*, 2022, **13**, 27.
13 P. Ares and K. S. Novoselov, *Nano Mater. Sci.*, 2022, **4**, 3–9.
14 D. Xu, Q. Zhang, X. Huo, Y. Wang and M. Yang, *Mater. Genome Eng. Adv.*, 2023, **1**, e11.
15 Y. Kang, L. Li and B. Li, *J. Energy Chem.*, 2021, **54**, 72–88.
16 H. Li, J. H. Lim, Y. Lv, N. Li, B. Kang and J. Y. Lee, *Chem. Rev.*, 2023, **123**, 4795–4854.
17 M. Golzani, A. Tadjarodi, M. Golzani, M. Poliki, R. Zare-Dorabei and K. Dashtian, *Coord. Chem. Rev.*, 2024, **510**, 215838.
18 T. He, Y. Kong, A. R. P. Santiago, M. A. Ahsan, H. Pan and A. Du, *Mater. Chem. Front.*, 2021, **5**, 6392–6412.
19 M. Garrido, L. Gualandi, S. Di Noja, G. Filippini, S. Bosi and M. Prato, *Chem. Commun.*, 2020, **56**, 12698–12716.
20 H. G. Ali, K. Khan, M. B. Hanif, M. Z. Khan, I. Hussain, M. S. Javed, H. A. AL-bonsrulah, M. Mosiałek, M. Fichtner and M. Motola, *J. Energy Storage*, 2023, **73**, 108980.

21 A. Balaban, C. C. Rentia and E. Ciupitu, *Rev. Roum. Chim.*, 1968, **13**, 231–247.
22 S. Berber, E. Osawa and D. Tománek, *Phys. Rev. B: Condens. Matter Mater. Phys.*, 2004, **70**, 085417.
23 R. Baughman, H. Eckhardt and M. Kertesz, *J. Chem. Phys.*, 1987, **87**, 6687–6699.
24 Q. Fan, L. Yan, M. W. Tripp, O. Krejč, S. Dimosthenous, S. R. Kachel, M. Chen, A. S. Foster, U. Koert and P. Liljeroth, *et al.*, *Science*, 2021, **372**, 852–856.
25 L. Hou, X. Cui, B. Guan, S. Wang, R. Li, Y. Liu, D. Zhu and J. Zheng, *Nature*, 2022, **606**, 507–510.
26 Q. Li, Y. Li, Y. Chen, L. Wu, C. Yang and X. Cui, *Carbon*, 2018, **136**, 248–254.
27 Y. Hu, C. Wu, Q. Pan, Y. Jin, R. Lyu, V. Martinez, S. Huang, J. Wu, L. J. Wayment and N. A. Clark, *et al.*, *Nat. Synth.*, 2022, **1**, 449–454.
28 V. G. Desyatkin, W. B. Martin, A. E. Aliev, N. E. Chapman, A. F. Fonseca, D. S. Galvão, E. R. Miller, K. H. Stone, Z. Wang and D. Zakhidov, *et al.*, *J. Am. Chem. Soc.*, 2022, **144**, 17999–18008.
29 S. He, B. Wu, Z. Xia, P. Guo, Y. Li and S. Song, *Nanoscale Adv.*, 2023, **5**, 2487–2492.
30 E. S. Penev, N. Marzari and B. I. Yakobson, *ACS Nano*, 2021, **15**, 5959–5976.
31 H. Geng, Y. Peng, L. Qu, H. Zhang and M. Wu, *Adv. Energy Mater.*, 2020, **10**, 1903030.
32 E. Pérez-Mayoral, I. Matos, M. Bernardo, M. Ventura and I. M. Fonseca, *Catalysts*, 2020, **10**, 1407.
33 M. Perovic, Q. Qin and M. Oschatz, *Adv. Funct. Mater.*, 2020, **30**, 1908371.
34 X.-L. Zhou, H. Zhang, L.-M. Shao, F. Lü and P.-J. He, *Waste Biomass Valorization*, 2021, **12**, 1699–1724.
35 R. Chakraborty, K. Vilya, M. Pradhan and A. K. Nayak, *J. Mater. Chem. A*, 2022, **10**, 6965–7005.
36 S. J. Clark, M. D. Segall, C. J. Pickard, P. J. Hasnip, M. I. Probert, K. Refson and M. C. Payne, *Z. Kristallogr. – Cryst. Mater.*, 2005, **220**, 567–570.
37 D. Systèmes, *San Diego*, 2017.
38 J. P. Perdew, K. Burke and M. Ernzerhof, *Phys. Rev. Lett.*, 1996, **77**, 3865.
39 J. Heyd, G. E. Scuseria and M. Ernzerhof, *J. Chem. Phys.*, 2003, **118**, 8207–8215.
40 J. D. Head and M. C. Zerner, *Chem. Phys. Lett.*, 1985, **122**, 264–270.
41 B. G. Pfrommer, M. Côté, S. G. Louie and M. L. Cohen, *J. Comput. Phys.*, 1997, **131**, 233–240.
42 M. Rizwan, A. Ayub, M. Shakil, Z. Usman, S. Gillani, H. Jin and C. Cao, *Mater. Sci. Eng., B*, 2021, **264**, 114959.
43 S. Nosé, *J. Chem. Phys.*, 1984, **81**, 511–519.
44 D. G. Sangiovanni, G. Gueorguiev and A. Kakanakova-Georgieva, *Phys. Chem. Chem. Phys.*, 2018, **20**, 17751–17761.
45 C. Lundgren, A. Kakanakova-Georgieva and G. K. Gueorguiev, *Nanotechnology*, 2022, **33**, 335706.
46 S. Plimpton, *J. Comput. Phys.*, 1995, **117**, 1–19.
47 A. V. Shapeev, *Multiscale Model. Simul.*, 2016, **14**, 1153–1173.
48 I. S. Novikov, K. Gubaev, E. V. Podryabinkin and A. V. Shapeev, *Mach. Learn. Sci. Technol.*, 2020, **2**, 025002.
49 G. Kresse and J. Furthmüller, *Phys. Rev. B: Condens. Matter Mater. Phys.*, 1996, **54**, 11169.
50 B. Mortazavi, F. Shojaei, F. Ding and X. Zhuang, *FlatChem*, 2023, **42**, 100575.
51 B. Mortazavi, M. Silani, E. V. Podryabinkin, T. Rabczuk, X. Zhuang and A. V. Shapeev, *Adv. Mater.*, 2021, **33**, 2102807.
52 B. Mortazavi, F. Shojaei, A. V. Shapeev and X. Zhuang, *Carbon*, 2022, **194**, 230–239.
53 B. Mortazavi, X. Zhuang, T. Rabczuk and A. V. Shapeev, *Mater. Horiz.*, 2023, **10**, 1956–1968.
54 B. Mortazavi, I. S. Novikov, E. V. Podryabinkin, S. Roche, T. Rabczuk, A. V. Shapeev and X. Zhuang, *Appl. Mater. Today*, 2020, **20**, 100685.
55 N. S. Martys and R. D. Mountain, *Phys. Rev. E: Stat. Phys., Plasmas, Fluids, Relat. Interdiscip. Top.*, 1999, **59**, 3733.
56 H. C. Andersen, *J. Chem. Phys.*, 1980, **72**, 2384–2393.
57 A. P. Thompson, S. J. Plimpton and W. Mattson, *J. Chem. Phys.*, 2009, **131**, 154107.
58 Z. Ni, H. Wang, J. Kasim, H. Fan, T. Yu, Y. H. Wu, Y. Feng and Z. Shen, *Nano Lett.*, 2007, **7**, 2758–2763.
59 W.-J. Yin, Y.-E. Xie, L.-M. Liu, R.-Z. Wang, X.-L. Wei, L. Lau, J.-X. Zhong and Y.-P. Chen, *J. Mater. Chem. A*, 2013, **1**, 5341–5346.
60 R. M. Tromer, M. L. Pereira Júnior, K. A. L. Lima, A. F. Fonseca, L. R. da Silva, D. S. Galvao and L. A. Ribeiro Junior, *J. Phys. Chem. C*, 2023, **127**, 12226–12234.
61 T. Jenkins, A. M. Silva, M. G. Menezes, T. Thonhauser and S. Ullah, *J. Phys. Chem. C*, 2024, **128**(26), 10982–10996.
62 S. Ullah, M. G. Menezes and A. M. Silva, *Carbon*, 2024, **217**, 118618.
63 Y. Luo, C. Ren, Y. Xu, J. Yu, S. Wang and M. Sun, *Sci. Rep.*, 2021, **11**, 19008.
64 J. Y. Jo and B. G. Kim, *Phys. Rev. B: Condens. Matter Mater. Phys.*, 2012, **86**, 075151.
65 R. M. Tromer, M. G. E. da Luz, M. S. Ferreira and L. F. C. Pereira, *J. Phys. Chem. C*, 2017, **121**, 3055–3061.
66 R. M. Tromer, L. D. Machado, C. F. Woellner and D. S. Galvao, *Phys. E*, 2021, **129**, 114586.
67 P. Rani, G. S. Dubey and V. Jindal, *Phys. E*, 2014, **62**, 28–35.
68 X. Cheng, N. Xiao, B. Zhou and B. Zhou, *Eur. Phys. J. Plus*, 2023, **138**, 437.
69 S. Lei, Q. Cao, X. Geng, Y. Yang, S. Liu and Q. Peng, *Crystals*, 2018, **8**, 465.
70 R. V. Mises, *Math.-phys. Klasse*, 1913, **4**, 582–592.
71 M. L. Pereira Junior, L. A. Ribeiro Junior, W. H. Brandão, A. L. Aguiar, D. S. Galvão and J. M. De Sousa, *Chem. Phys. Chem.*, 2020, **21**, 1918–1924.
72 M. L. P. Júnior and L. A. R. Júnior, *FlatChem*, 2020, **24**, 100196.
73 M. Pereira, W. Da Cunha, R. De Sousa, G. A. Nze, D. Galvão and L. Ribeiro, *Nanoscale*, 2022, **14**, 3200–3211.